Earth and Planetary Science Letters 467 (2017) 1–9

Contents lists available at ScienceDirect

Earth and Planetary Science Letters

www.elsevier.com/locate/epsl

A long history of equatorial deep-water upwelling in the Pacific Ocean

Yi Ge Zhang [a,b,c,*], Mark Pagani [b], Jorijntje Henderiks [d], Haojia Ren [e]

[a] Department of Oceanography, Texas A&M University, College Station, TX 77843, United States
[b] Department of Geology and Geophysics, Yale University, New Haven, CT 06511 United States
[c] Department of Earth and Planetary Sciences, Harvard University, Cambridge, MA 02138, United States
[d] Department of Earth Sciences, Uppsala University, SE-75 236 Uppsala, Sweden
[e] Department of Geosciences, National Taiwan University, Taipei, Taiwan, ROC

ARTICLE INFO

Article history:
Received 7 July 2016
Received in revised form 1 March 2017
Accepted 9 March 2017
Available online xxxx
Editor: M. Frank

Keywords:
alkenone-pCO_2
deep-water upwelling
eastern equatorial Pacific
late Miocene – early Pliocene "biogenic bloom"

ABSTRACT

Cold, nutrient- and CO_2-rich waters upwelling in the eastern equatorial Pacific (EEP) give rise to the Pacific cold tongue. Quasi-periodic subsidence of the thermocline and attenuation in wind strength expressed by El Niño conditions decrease upwelling rates, increase surface-water temperatures in the EEP, and lead to changes in regional climates both near and far from the equatorial Pacific. EEP surface waters have elevated CO_2 concentrations during neutral (upwelling) or La Niña (strong upwelling) conditions. In contrast, approximate air–sea CO_2 equilibrium characterizes El Niño events. One hypothesis proposes that changes in physical oceanography led to the establishment of a deep tropical thermocline and expanded mixed-layer prior to 3 million years ago. These effects are argued to have substantially reduced deep-water upwelling rates in the EEP and promoted a "permanent El Niño-like" climate state. For this study, we test this supposition by reconstructing EEP "excess CO_2" and upwelling history for the past 6.5 million years using the alkenone-pCO_2 methodology. Contrary to previous assertions, our results indicate that average temporal conditions in the EEP over the past ~6.5 million years were characterized by substantial CO_2 disequilibrium and high nutrient delivery to surface waters — characteristics that imply strong upwelling of deep waters. Upwelling appears most vigorous between ~6.5 to 4.5 million years ago coinciding with high accumulation rates of biogenic material during the late Miocene – early Pliocene "biogenic bloom".

1. Introduction

The eastern equatorial Pacific (EEP) is one of the most dynamic regions in the world ocean. Wind-driven upwelling in the EEP brings cold, nutrient- and CO_2-rich deep-waters to the surface, setting up east–west gradients in a number of parameters including sea surface temperature (SST), export production and surface seawater CO_2 (Feely et al., 2002; Fiedler and Talley, 2006; Keeling, 1968). However, quasi-periodic (2–7 years) ocean–atmosphere perturbations of El Niño – Southern Oscillation (ENSO) significantly reduce deep-water upwelling in the EEP by deepening the thermocline, which impacts regional and global climates and the carbon cycle (McPhaden et al., 2006).

One supposition suggests that, prior to 3 million years ago (Ma), the equatorial Pacific Ocean maintained a negligible zonal temperature gradient similar to modern El Niño conditions, often referred to as the "permanent El Niño" hypothesis (Fedorov et al., 2013). During the "permanent El Niño-like" interval, the EEP is thought to have had a deep thermocline and near absence of deep-water upwelling (Fedorov et al., 2006; Philander and Fedorov, 2003). Subsequent global cooling and shoaling of the tropical thermocline would have promoted equatorial upwelling, the appearance of cold EEP sea surface temperatures (SSTs), and the eventual establishment of modern zonal temperature gradients (Fedorov et al., 2006; Philander and Fedorov, 2003). Evidence for near cessation of upwelling in the EEP region before 3 Ma is inferred from SST reconstructions that indicate substantially higher temperatures during the Miocene – Pliocene in many coastal and equatorial upwelling regions (Brierley et al., 2009; Rommerskirchen et al., 2011; Rosell-Mele et al., 2014), including the EEP (Dekens et al., 2007; Lawrence et al., 2006; Rousselle et al., 2013; Zhang et al., 2014). Recent biomarker-based temperature reconstructions indicate that the western equatorial Pacific (WEP) was also warmer, maintaining a zonal SST gradient in the tropical Pacific throughout the late Miocene – Pliocene (O'Brien et al., 2014; Zhang et al., 2014). However, the Pacific zonal temperature gradient was about ~3–4 °C during 12–3 Ma, reduced relative to the average late Quaternary

* Corresponding author at: Department of Oceanography, Texas A&M University, College Station, TX 77843, United States.
E-mail address: yige.zhang@tamu.edu (Y.G. Zhang).

http://dx.doi.org/10.1016/j.epsl.2017.03.016
0012-821X/

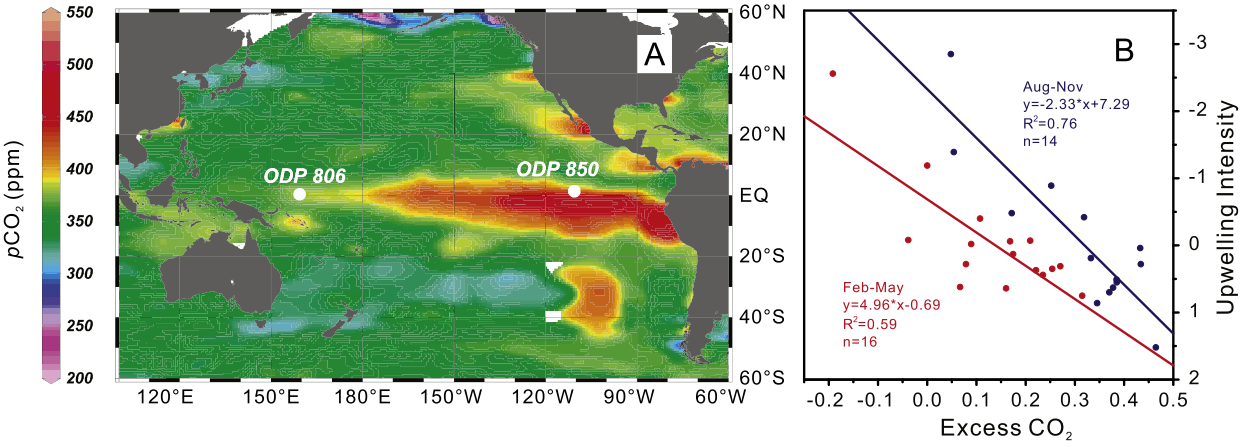

Fig. 1. Sample site locations and modern seawater pCO_2 relationships. (A), Surface seawater pCO_2 measurements collected 1957–2012 (Takahashi and Sutherland, 2012). Weighted-average gridding by Ocean Data View; ppm = parts per million. (B), Excess seawater CO_2 near ODP Site 850 relative to equilibrium conditions and "upwelling intensity" scaled by the Nino 3 index values. Regressions were performed using seasonal data from August to November and February to May. The t values for the two regressions are −4.8 and −6.5, respectively. At 0.05 level, both slopes are significant from zero. No data are available for December and January.

values (∼5 °C) (Zhang et al., 2014). Importantly, the temporal resolution of deep-sea sediments does not allow the determination of the actual interannual climate variability, and new model simulation argues against using ENSO as analogs for long-term changes in tropical conditions (DiNezio et al., 2010).

Deep-sea sediment cores in the EEP consistently show that the mass accumulation rate (MAR) of biogenic components, such as carbonate and opal derived from marine microplankton, was significantly elevated during the late Miocene – early Pliocene, suggesting high export production in this region that probably links to the nutrient influx brought by deep-water upwelling (Farrell et al., 1995; Ma et al., 2015; Reghellin et al., 2015; Shackleton and Hall, 1995). The warm SSTs and high export production in the EEP during the "permanent El Niño-like" period appears to provide conflicting evidence for the strengths of equatorial upwelling.

It has been shown that the carbon cycle could be more sensitive to deep-water upwelling than temperature (Keller et al., 2015). Specifically, the outcrop of deep-water is usually associated with the outgassing of excess CO_2 accumulated from remineralization processes in seawater (Feely et al., 2002). In this study, we present surface seawater CO_2 levels in the western and eastern equatorial Pacific. Assuming the pCO_2 at WEP maintains approximate air–sea equilibrium, the WEP and EEP records are used together to compute the "excess CO_2" in the EEP, an independent proxy to probe the history of equatorial deep-water upwelling since the late Miocene.

2. Background

Deep-water upwelling in the EEP maintains air–sea CO_2 disequilibrium representing the world's largest ocean-to-atmosphere CO_2 flux (Takahashi et al., 2009) (Fig. 1). Pacific equatorial thermocline waters are sourced from the subduction of surface seawater in the extratropics — primarily in the Southern Hemisphere including Subantarctic Mode Water, but also in the Northern Hemisphere (O'Connor et al., 2002) — and are eventually transported by the Equatorial Undercurrent to the EEP. During neutral or La Niña conditions, pCO_2 in EEP surface waters can be ∼50% higher than equilibrium conditions (Feely et al., 2002). During El Niño events, the thermocline deepens, surface water warms, and strong air–sea CO_2 disequilibrium quickly vanishes – a pattern that was revealed by the ship-board surveys during the 1994 and 1998 El Niño events (Feely et al., 2002). Long-term observations confirm the dominant influence of decadal-timescale ENSO phases on surface-seawater pCO_2, superimposed on the trend of anthropogenic CO_2 increase (Sutton et al., 2014). This implies that ancient pCO_2 levels recorded by sediments could be used to probe past deep-water upwelling strengths in this region (cf. Martinez-Boti et al., 2015; Palmer and Pearson, 2003).

Upwelling intensity in the equatorial Pacific is related to Ekman mass transport determined by the Coriolis parameter and wind stress, the history of which is lacking over the past several decades. Alternatively, wind stress, temperature and upwelling intensity are directly coupled on seasonal timescales in the EEP via the Bjerknes feedback (Bjerknes, 1969) which is captured in records of Nino 3 – an index that represents the magnitude of temperature anomalies in the EEP. Thus, the Nino 3 index acts as a proxy for upwelling intensity in the EEP on a seasonal timescale. Indeed, seawater pCO_2 measurements (Bakker et al., 2014) between years 1992 and 2007 in the vicinity of Ocean Drilling Program (ODP) Site 850 (Fig. S1) show that excess CO_2 (i.e., $[pCO_{2(sw)}/pCO_{2(air)}]-1$) and the degree of upwelling intensity, determined from Nino 3 values, are correlated (Fig. 1B). In contrast, the modern western Pacific warm pool is characterized by a deep mixed-layer and relative air–sea CO_2 equilibrium (Fig. 1A). Consequently, sea-surface pCO_2 offsets between the EEP (Site 850) and WEP (Site 806, Fig. 1A) provide a measure of excess CO_2 in the EEP through time.

We evaluated the magnitude of regional air–sea CO_2 disequilibrium across the equatorial Pacific Ocean for the past ∼6.5 million years using the alkenone-CO_2 approach. Alkenones are long-chained (C_{37} to C_{39}) unsaturated ethyl and methyl ketones produced by haptophyte algae in the modern ocean (Conte et al., 1995). Alkenone-CO_2 reconstructions derive from the stable carbon-isotope composition of the di-unsaturated C_{37} methyl ketone ($\delta^{13}C_{37:2}$), planktonic foraminifera ($\delta^{13}C_{PF}$) and the total carbon isotope fractionation during algal growth ($\varepsilon_{p37:2}$). The magnitude of $\varepsilon_{p37:2}$ is a function of extracellular aqueous CO_2 concentration ($[CO_{2(aq)}]$), growth rate (μ), and cell geometry (i.e., the ratio of cellular volume to surface area), among other factors (Freeman and Pagani, 2005; Pagani, 2014). The phytoplankton physiological parameters such as growth rate and light availability are usually simplified to a single term 'b', estimated from the concentration of reactive soluble phosphate ($[PO_4^{3-}]$) (Bidigare et al., 1997) or export productivity (Seki et al., 2010). We adopt the phosphate–b relationship from the global or regional survey of suspended particles to estimate modern b value at both sites. $\varepsilon_{p37:2}$ values were established at Site 850, while an existing Pliocene record (Pagani et al., 2010) was extended to the late Miocene at Site 806 (Fig. 2A, S2).

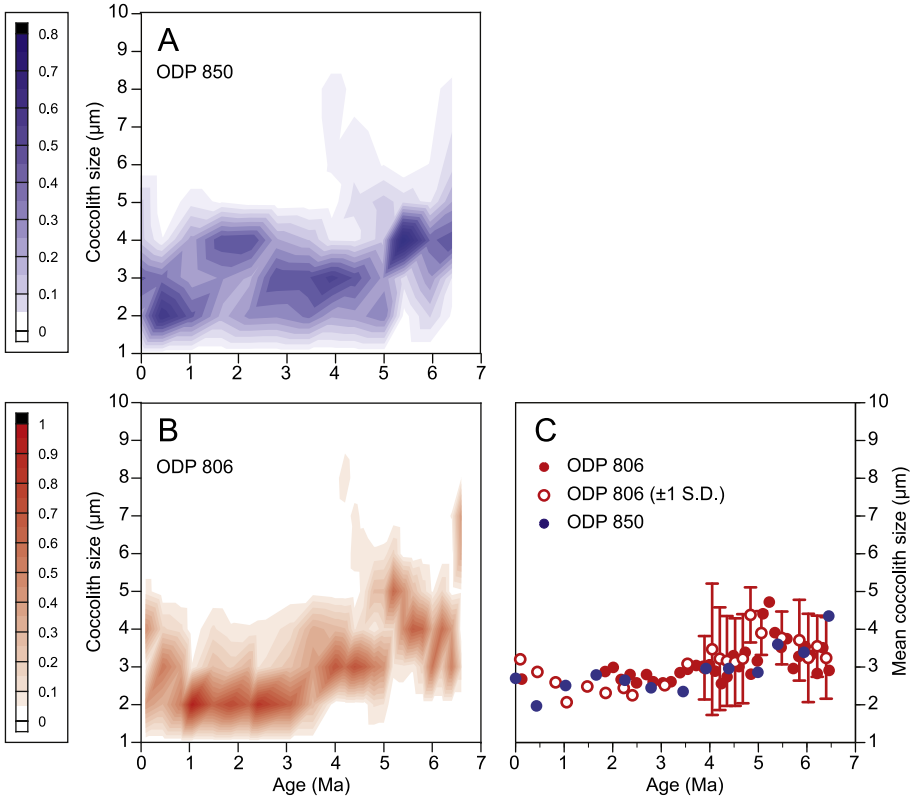

Fig. 2. Noelaerhabdaceae coccolith size at ODP Sites 806 and 850. (A), (B), Contour plots of size distributions show similar temporal size trends for ancient alkenone-producing coccolithophores at each respective site. (C), Mean coccolith size remained highly comparable between the EEP and equatorial Pacific warm pool over the studied time interval. Results are based on assemblage counts (solid circles, Site 806 (Sucheras-Marx and Henderiks, 2014; Takayama, 1993); Site 850: this study) as well as coccolith biometry (hollow circles, Site 806, mean ±1S.D.; this study).

3. Material and methods

3.1. Study sites and sample processing

ODP Site 806 (0°19.11′N, 159°21.69′E, water depth 2520 m) was drilled on Ontong Java Plateau in the western equatorial Pacific. Hole 806B sediments are comprised of foraminifer nannofossil ooze and chalk to nannofossil ooze and chalk with foraminifers (Shipboard Scientific Party, 1991). The age model for Site 806 applies an integration of calcareous nannofossils (Takayama, 1993) and planktonic foraminifer (Chaisson and Leckie, 1993) biostratigraphy that is updated to the GTS 2004 timescale (Nathan and Leckie, 2009). The upper ~200 m of sediment represent the most recent 6.53 Ma. Site 850 (1°17.83′N, 110°31.29′W, water depth 4197 m) is one of the sites in the eastern equatorial transect of ODP Leg 138. Hole 850B is composed of nannofossil ooze with varying proportions of other microfossil-derived constituents such as opal (Shipboard Scientific Party, 1992). The age model for Site 850 is determined by biostratigraphy and magnetostratigraphy (Baldauf and Iwai, 1995; Raffi and Flores, 1995; Shackleton et al., 1995). Key geomagnetic reversal boundaries and biohorizons are revised to reflect the updated GTS 2004 timescale (Reghellin et al., 2015). The upper 221.62 m of sediment represent the most recent 7.07 Ma.

Approximately 50 cm^3 of sediments were freeze-dried and homogenized with a mortar and pestle, and then extracted using a Dionex accelerated solvent extractor (ASE) 300 with 2:1 (v/v) dichloromethane/methanol, at 120 °C and 10.3 MPa for 16 min per sample. Total Lipid Extracts (TLEs) were then concentrated under a stream of purified N_2 and separated into compound fractions using silica-gel chromatography. Ashed Pasteur pipettes loaded with approximately 0.5 g deactivated silica gel were sequentially treated with 2 ml hexane, 4 ml dichloromethane and 4 ml of methanol to obtain aliphatic (S1), aromatic (S2) and polar fractions (S3), respectively. Alkenones eluted in the S2 fraction (Zhang et al., 2014). Planktonic foraminifera *Globigerinoides sacculifer* were picked from the >250 μm size fraction using ~10 g of sediment rinsed with deionized water.

3.2. Stable isotope analyses

The ketone fraction was first analyzed on a Thermo Trace 2000 Gas Chromatography (GC) equipped with a Restek DB-1 capillary column (60 m × 0.25 mm × 0.25 μm), a Programmable Temperature Vaporization (PTV) injector and a Flame Ionization Detector (FID). The oven was set to 90 °C upon sample injection, held for 1 min, ramped up at 20 °C min^{-1} to 280 °C, then 2 °C min^{-1} to 320 °C. Temperature was held constant at 320 °C for 30 min. Heptatriaconta-15E, 22E-dien-2-one (di-unsaturated alkenone) was identified by comparison of elution times with known alkenone standards. Relative abundances of $C_{37:2}$ and $C_{37:3}$ alkenone were quantified to calculate $U^{K'}_{37}$ indices and SSTs, which was previously reported (Zhang et al., 2014). Carbon isotope compositions of alkenones were analyzed on a Thermo Finnigan MAT 253 mass spectrometer interfaced with a Trace GC Combustion III (GC-IRMS). The GC was equipped with a PTV injector and a Restek column, with the set up similar to above described $U^{K'}_{37}$ analyses. Carbon isotopic signatures are reported relative to the VPDB standard based on an in-house reference gas calibrated to the OzTech standard ($\delta^{13}C = -40.61‰$). A *n*-C_{38} ($\delta^{13}C = -29.33‰$) and *n*-C_{41} ($\delta^{13}C = -28.78‰$) alkane standard was co-injected with every measurement and used to correct $\delta^{13}C$ values of alkenones. Most samples were measured in duplicate or triplicate, for alkenone $\delta^{13}C$ ($\delta^{13}C_{37:2}$) and the average standard

error = ±0.31‰ for Site 850, and ±0.30‰ for Site 806 samples. $\delta^{13}C$ values of the $C_{37:2}$ alkenone and the planktonic foraminifera *Globigerinoides sacculifer* were used to compute $\varepsilon_{p37:2}$. The $\delta^{13}C_{37:2}$ record at Site 806 between 5–0 Ma was previously published (Pagani et al., 2010).

~200 mg foraminifera tests were acidified by 105% phosphoric acid at 25 °C overnight. CO_2 generated from acidification was measured for $\delta^{13}C$ and $\delta^{18}O$ using Thermo DeltaPlus XP mass spectrometer equipped with a GasBench interface. NBS 19 and two in-house standards were used. Accuracy for NBS 19 is 0.13‰ for $\delta^{13}C$ and 0.24‰ for $\delta^{18}O$. Planktonic foraminiferal carbon isotopes ($\delta^{13}C_{PF}$) were used to calculated $\delta^{13}C$ of dissolved CO_2, assuming equilibrium fractionations at proxy-reconstructed temperatures.

3.3. Coccolith biometry

Coccolith size is a useful proxy to evaluate the impacts of algal cell geometry on the alkenone-pCO_2 methodology (Henderiks, 2008; Henderiks and Pagani, 2007). Here, we examine if paleoenvironmental gradients between the EEP and WEP are also reflected by fossil assemblages of ancient alkenone producers (family Noelaerhabdaceae: *Reticulofenestra* spp., *Gephyrocapsa* spp. and *E. huxleyi*). The variation in coccolith size was determined in two ways using polarized light microscopy. First, biometry of randomly chosen, individual coccoliths (with $N \geq 40$ up to 140) gives accurate estimates for mean size (maximum diameter or length, L), its standard variation (S.D.) and the overall size distribution (Henderiks and Pagani, 2007). Second, assemblage counts (>300 specimens per sample) of the same coccolithophore group were used to derive overall size distributions (relative frequency, f/n of size-defined categories, set at 1–2 µm bins) and calculate a mean size estimate for each sample, as follows:

$$\sum_{i=1}^{n}(f/n_i \times L_i) \tag{1}$$

where L denotes the mid-range value (in µm) of each bin. Both approaches give highly comparable results for our purpose to compare temporal trends in both the means and overall size distributions between Sites 850 and 806 (Fig. 2).

3.4. pCO_2

Ancient levels of CO_2 were calculated using the equation (Bidigare et al., 1997; Jasper et al., 1994; Pagani, 2014)

$$\varepsilon_{p37:2} = \varepsilon_f - \frac{b}{[CO_{2(aq)}]} \tag{2}$$

where $\varepsilon_{p37:2}$ is the total carbon isotope fractionation that occurs during algal photosynthesis, and ε_f represents the carbon isotope fractionations associated with the enzymes Rubisco (ribulose-1,5-bisphosphate carboxylase oxygenase) and β-carboxylase (phosphoenolpyruvate-carboxylase) (Goericke et al., 1994). A value of 25‰ was assumed for ε_f. The term 'b' integrates all physiological variables affecting the total carbon isotope fractionation during photosynthesis. Global survey of $\varepsilon_{p37:2}$ using suspended particles in seawater indicate that b is related to $[PO_4^{3-}]$ (Bidigare et al., 1997; Eek et al., 1999; Laws et al., 2001; Popp et al., 1999), which yields a b–$[PO_4^{3-}]$ relationship (Pagani et al., 2005) that is commonly used by alkenone-CO_2 reconstructions and applied to Site 806 in this study. For the EEP, however, an adequate amount of modern data is available which enabled us to develop and apply a regional b–$[PO_4^{3-}]$ relationship to Site 850 ($n = 33$, $r^2 = 0.95$):

$$b = 154.14 \times \left[PO_4^{3-}\right] + 44.04 \tag{3}$$

$U^{K'}_{37}$ and TEX_{86} indices provided SST estimates at both sites (Zhang et al., 2014) and subsequently applied to calculate $\varepsilon_{p37:2}$ and $[CO_{2(aq)}]$. pCO_2 reconstructions represent theoretically equilibrated values calculated using Henry's Law. These procedures were applied to the newly generated $\varepsilon_{p37:2}$ records from Site 850 (0–6.5 Ma), Site 806 (5–6.5 Ma) as well as the previously published $\varepsilon_{p37:2}$ record for Site 806 (0–5 Ma) (Pagani et al., 2010) to calculate pCO_2.

4. Results and discussions

4.1. $\varepsilon_{p37:2}$

Our results show that $\varepsilon_{p37:2}$ values at Site 850 between 6.5 to 5 Ma are similar and/or slightly higher than $\varepsilon_{p37:2}$ values at Site 806. At Site 850, $\varepsilon_{p37:2}$ decreases from ~6.5 to 4 Ma to values generally lower than those measured in the western warm pool. At Site 806, a slight trend toward lower $\varepsilon_{p37:2}$ values begins at 3 Ma (Fig. 3A). Morphometric analysis of coccoliths derived from alkenone-producing coccolithophores (*Reticulofenestra, Gephyrocapsa* and *Emiliania*) reveal similar cell size dimensions and changes at both sites over the past ~6.5 million years (Fig. 2), leaving haptophyte growth rates and/or surface $[CO_{2(aq)}]$ as likely factors driving the character of equatorial Pacific $\varepsilon_{p37:2}$ values.

Relatively lower $\varepsilon_{p37:2}$ values at Site 850 (Fig. 3A) could have resulted from lower surface-water $[CO_{2(aq)}]$ and/or higher haptophyte growth rates (µ) in the EEP relative to the western warm pool. In the modern ocean, µ, nutrient levels, and surface $[CO_{2(aq)}]$ are all elevated along low-latitude upwelling systems, such as the Peru margin (Bidigare et al., 1997). Modern $\varepsilon_{p37:2}$ values from the Peru Margin upwelling system are very low (average $\varepsilon_{p37:2}$ = 8.9‰), reflecting the influence of haptophyte growth rates, as well as a high surface-water $[PO_4^{3-}]/[CO_{2(aq)}]$ ratio (Fig. S3) (Bidigare et al., 1997). Similarly, low $\varepsilon_{p37:2}$ values driven by high haptophyte growth rates also characterize surface sediments collected in the Angola and Benguela coastal upwelling regions in the South Atlantic Ocean (Benthien et al., 2002). Consequently, the appearance of comparatively low $\varepsilon_{p37:2}$ values at Site 850 relative to Site 806 over the past 5 million years probably reflect high nutrient conditions and haptophyte growth rates in the EEP.

Between ~6.5–5 Ma, $\varepsilon_{p37:2}$ values could reflect the absence of a nutrient and growth rate gradient between Sites 850 and 806 due to a cessation of upwelling in the EEP (Fig. 2B). Available primary productivity indicators from Site 850, however, argue against this assertion. Mass accumulation rates (MARs) of biogenic opal produced by siliceous plankton including diatoms and radiolarians were exceptionally high between ~7 to 4.5 Ma at Site 850 (Farrell et al., 1995). High export production is further supported by the elevated MAR of barium (primarily as barite, $BaSO_4$), an independent productivity indicator that is more resistant to post-depositional dissolution (Schroeder et al., 1997). Opal MARs from the equatorial transect sites (849, 850, 851) in the upwelling region suggest enhanced nutrient supply and export production is widely distributed in the EEP, with the interval between 7 to 4.5 Ma termed the late Miocene – early Pliocene "biogenic bloom" (Farrell et al., 1995). Sites 849, 850 and 851 crossed the equator by ~0 Ma, 4 Ma and >9 Ma (Shipboard Scientific Party, 1992), suggesting that the synchronous increase in export productivity was not a consequence of site position due to plate tectonic changes (Farrell et al., 1995; Reghellin et al., 2015).

Biogenic carbonate MARs also indicate that export production at Site 806 was elevated during the "biogenic bloom". However, unlike Site 850 where diatoms comprised up to 75% of the sediment in the late Miocene section (Farrell et al., 1995), siliceous sedimentation at Site 806 represents a minor component (<5%) throughout the studied interval (Shipboard Scientific Party, 1991),

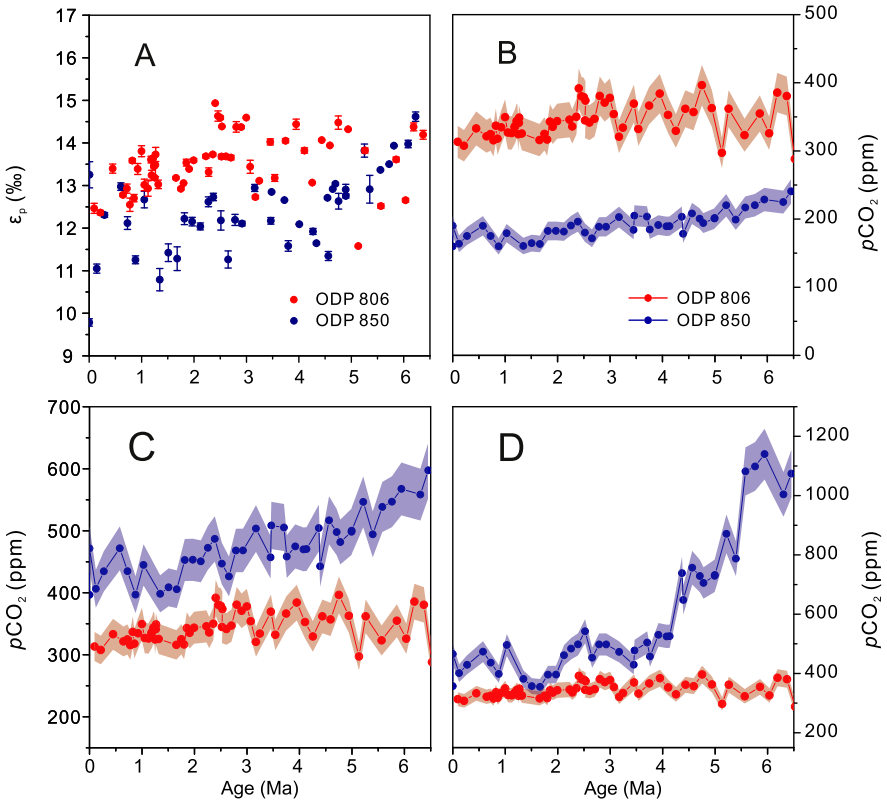

Fig. 3. $\varepsilon_{p37:2}$ and pCO_2 reconstructions for surface seawater. (A), $\varepsilon_{p37:2}$ values were calculated from the carbon isotopic compositions of heptatriaconta-15E, 22E-dien-2-one and *Globigerinoides sacculifer* (Fig. S2). Reconstructions of pCO_2 (panels B, C, D) calculated from $\varepsilon_{p37:2}$ assume: (B), identical $[PO_4^{3-}]$ at Sites 850 and 806. This assumes both sites were characterize by modern values of subsurface $[PO_4^{3-}]$ measured at Site 806 of 0.16 μM; (C), modern $[PO_4^{3-}]$ distribution at Sites 806 (0.16 μM) and 850 (0.82 μM) respectively. (D), variable physiological parameter *b* at Sites 806 and 850 assuming changes in *b* are directly proportional to changes in the MAR of $CaCO_3$ (Lyle, 2003). Error bands of pCO_2 estimates reflect the Monte Carlo propagated uncertainty (±7.5%), considering the errors associated with isotope analyses, the *b*–$[PO_4^{3-}]$ relationship, SSTs estimates, salinity and ε_f (Pagani et al., 1999). Note: scales of y-axis differ for each panel.

implicating different nutrient regimes at Sites 850 and 806. Thus, available data indicate that a zonal equatorial nutrient gradient persisted for at least the past 6.5 million years, and that pCO_2 reconstructions based on the assumption that low $[PO_4^{3-}]$ distributions characterized both sites are unsupported (Fig. 3B).

4.2. Choices of 'b' for pCO_2 calculations

Theoretically, values of the physiological factor '*b*' can be adjusted relative to changes in cell size of ancient haptophytes (Henderiks and Pagani, 2007). Such "cell size correction" would result, for both sites, in a slight attenuation of the reconstructed pCO_2 values. However, we refrained from these corrections to our pCO_2 reconstructions in Fig. 3 and focus our discussion on the relative differences in $[PO_4^{3-}]$ and regional export production. The reasons are twofold: (a) haptophyte cell size and growth rates are interdependent. Therefore, correcting CO_2 using only one variable without accounting for the other would result in unrealistic CO_2 estimates; (b) any cell size correction should not change the difference between pCO_2 estimated from Sites 806 and 850, since the cell size evolution from both sites are tracking each other (Fig. 2C).

The variations of algal growth rate at Sites 806 and 850 over the past 6.5 million years are critical for pCO_2 estimates. Previously, variables linked to export production have been used to approximate for *b* changes (e.g., Seki et al., 2010), although productivity and phytoplankton growth rate could be decoupled in certain cases (Goericke and Welschmeyer, 1998). Developing an accurate and vastly applicable productivity proxy is a challenge, evidenced by the recent proxy calibration in the North Pacific which showed region-dependent correspondence between export production and opal and Ba flux (Serno et al., 2014). Nonetheless, uniformly increased mass accumulation rates (MARs) of opal, calcium carbonate (Farrell et al., 1995) and Ba (Schroeder et al., 1997) across several sites in the EEP (ODP Sites 849, 850, 851) during the late Miocene – early Pliocene provide unambiguous evidence for elevated export production in this region. In the western equatorial Pacific, the available indicator of export production, MARs of calcium carbonate (Lyle, 2003), suggest that productivity was also enhanced during the Miocene–Pliocene.

Total organic carbon (TOC) or biomarkers (e.g., alkenones) linked to primary productivity are often used to scale for export production. Unlike carbonate or opal, which are the major constituents of deep-sea sediments, most of the organic carbon produced in the photic zone is degraded in the water column or in sediments at or near the seafloor, leaving a very small fraction preserved. For example, a study from the Arabian Sea showed that from sediment traps at 2200 m water depth to surface sediment (3974 m), only 0.8% of the alkenones and 3.3% of the TOC were preserved (Prahl et al., 2000). One can imagine that modest perturbations in the degradation process could largely affect the abundance and accumulation rate of organic material, substantially weakening the linkage between MARs of alkenones or TOC and export production (Prahl et al., 2000). We therefore refrained from using them to estimate pCO_2 changes.

At Site 850, export production has been evaluated by several proxies such as opal, $CaCO_3$ (Farrell et al., 1995) and Ba (Schroeder et al., 1997). In the western Pacific Site 806, calcium carbonate (Lyle, 2003) is the only proxy available to assess productivity changes. Therefore, we used calcium carbonate MARs at both Site

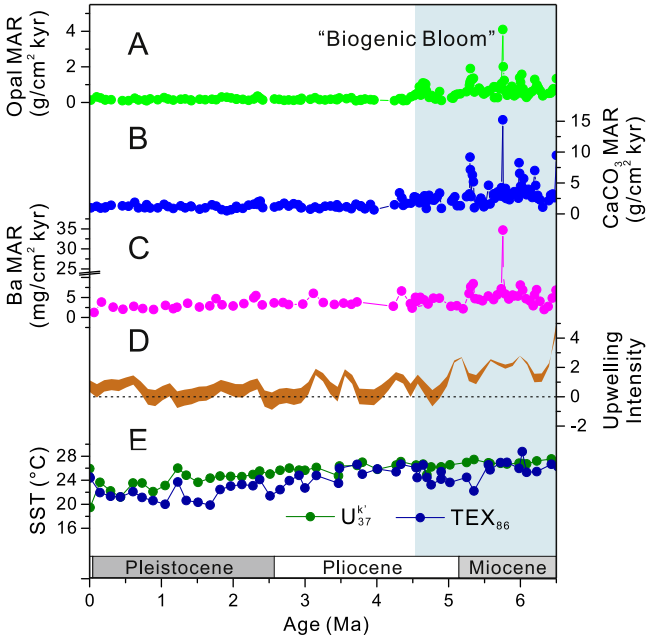

Fig. 4. Relationship between productivity, upwelling rates and temperature at EEP Site 850. A–C, mass accumulation rate of opal, $CaCO_3$ (Farrell et al., 1995) and Ba (Schroeder et al., 1997). (D), relative upwelling intensity, a dimensionless unit calculated using "excess CO_2" derived from Fig. 3C and the excess CO_2–upwelling intensity relationships derived from modern data near Site 850 (Fig. 1B). The dashed line indicates modern day averaged condition. (E), SSTs determined by two organic proxies TEX_{86} and $U^{K'}_{37}$ (Zhang et al., 2014). The temporal section highlighted in blue represents the period known as the late Miocene – early Pliocene "biogenic bloom". (For interpretation of the references to color in this figure legend, the reader is referred to the web version of this article.)

806 and 850 to scale for changes in b and computed pCO_2 accordingly.

$CaCO_3$ as an export production proxy could be complicated by the fact that calcium carbonate is easily subject to dissolution effects. However, two lines of evidence suggest that carbonate MARs can be used for Sites 806 and 850 on the studied timescale (0–6.5 Ma): (1) studies on bulk carbonate or calcareous nannofossils and foraminifera suggest no severe dissolution at both sites (Farrell et al., 1995; Lyle, 2003; Reghellin et al., 2015; Shipboard Scientific Party, 1991, 1992); and (2) the good correlations between calcium carbonate and opal and Ba at Site 850 (Fig. 4) indicate a primary productivity control on all three variables.

Apparently, the absolute MARs of $CaCO_3$ at different sites are not directly proportional to productivity, exemplified by the fact that carbonate MAR at Site 806 is higher than Site 850 during the late Quaternary (Fig. S4). This is a result of different water depths and much higher opal content Site 850 due to diatom blooms characteristic of high productivity regions. We therefore used modern $[PO_4^{3-}]$ levels to define b values at Sites 806 and 850, then utilized the changes in carbonate MAR relative to the late Quaternary level to scale for b changes.

If modern $[PO_4^{3-}]$ distributions are applied to $\varepsilon_{p37:2}$ values, reconstructed pCO_2 at Site 850 is always higher than Site 806 (Fig. 3C), with a secular decrease in the zonal CO_2 gradient with time. If we assume the physiological parameter b at Sites 806 and 850 varied directly proportional to changes in $CaCO_3$ MAR (Fig. S4), elevated biogenic material MARs in the late Miocene – Pliocene would increase the pCO_2 estimates at both Sites 850 and 806. Nonetheless, a large CO_2 asymmetry still existed during the late Miocene – early Pliocene (Fig. 3D).

In both scenarios, pCO_2 records from Site 806, presumably representing air–sea equilibrium, show a substantial CO_2 drop from ~6.5 Ma towards the present, ranging from ~50 ppm if the term b is assumed constant, to ~150 ppm if b varies proportionally to carbonate MAR (Fig. S5).

In the modern EEP, nutrients in upwelled waters are not fully consumed by phytoplankton as a result of iron (Fe) limitation (Coale et al., 1996). The flux of eolian material, an indicator of Fe input associated with mineral dust peaked during the late Miocene and decreased towards the present (Hovan, 1995), suggesting that the late Miocene – early Pliocene biogenic bloom could be explained simply by increased Fe supply. Mesoscale Fe fertilization experiments in the EEP showed increased productivity and phytoplankton growth rates after $FeSO_4$ addition (Bidigare et al., 1999). However, during these experiments, the algal biomarkers were also substantially ^{13}C-enriched due to elevated growth rate, resulting in low ε_p values (Bidigare et al., 1999). This contradicts the trend at Site 850 where $\varepsilon_{p37:2}$ values are higher in the late Miocene (Fig. 3A). Thus, our $\varepsilon_{p37:2}$ data argues against a decoupling of upwelling and primary production rates in this region for the past 6.5 million years.

4.3. "Upwelling intensity" of the EEP

pCO_2 estimates from Sites 806 and 850 assuming modern distribution of $[PO_4^{3-}]$ (Fig. 3C) were used to compute "excess CO_2", which is equivalent to $(pCO_{2(850)}/pCO_{2(806)}) - 1$. Excess CO_2 data were then used to estimate upwelling intensity, utilizing the modern excess CO_2–upwelling intensity relationships established based on the excess CO_2 data measured in the vicinity of Site 850 between 1992–2007 (Bakker et al., 2014) (Fig. S1), and Nino 3 index values (http://www.cpc.ncep.noaa.gov/data/indices/) times -1 to link stronger upwelling with positive values. Upwelling intensity $= 2.33 \times$ excess $CO_2 - 7.29$ for Aug–Nov, and $= -4.96 \times$ excess $CO_2 + 0.69$ for Feb–May (Fig. 1B). Seasonal excess CO_2–upwelling intensity relationships define the range of the upwelling intensity data presented in Fig. 3D.

Our results show substantially increased upwelling intensity during the late Miocene – early Pliocene at Site 850, consistent with export productivity proxies established from the same site, such as MARs of $CaCO_3$, opal (Farrell et al., 1995) and Ba (Schroeder et al., 1997). Upwelling intensity decreased in the Pliocene, with conditions similar to the modern established during the mid-Pliocene (Fig. 4D). Importantly, this conclusion is independent of export productivity changes in the EEP, since a conservative pCO_2 scenario based on the assumption that 'b' does not change over time (Fig. 3C) was used. If the CO_2 estimates derived from the carbonate MAR-scaled b are used, the late Miocene – early Pliocene upwelling intensity would be even more elevated because "excess CO_2" is larger in this scenario (Fig. 4D).

The persistence of warm EEP SSTs in the Miocene – Pliocene (Fig. 4E) suggests that mixed-layer temperature is not an adequate indicator of upwelling intensity over geological timescales. The decoupling between ocean temperature and export production has been previously noticed in the EEP (Dekens et al., 2007; Reghellin et al., 2015). However, surface (Dekens et al., 2007) and subsurface warming (Ford et al., 2012) in the EEP was interpreted as evidence of a considerable deepening of the thermocline in the Pliocene, which implies that the upwelling was restricted to mixed-layer waters without involvement of deeper thermocline waters (Dekens et al., 2007). However, warm surface/subsurface water temperatures do not always correlate with a downward movement of the thermocline. Operationally, the presence of the modern thermocline can be easily identified by a fixed temperature, for example, 13 °C (e.g., Deutsch et al., 2014). In contrast, during the Pliocene, the entire water column in the EEP — surface (Dekens et al., 2007; Lawrence et al., 2006; Rousselle et al., 2013; Zhang et al., 2014), subsurface (Ford et al., 2012), and bottom waters (Lear et al., 2015) — was warmer than the present, so that the

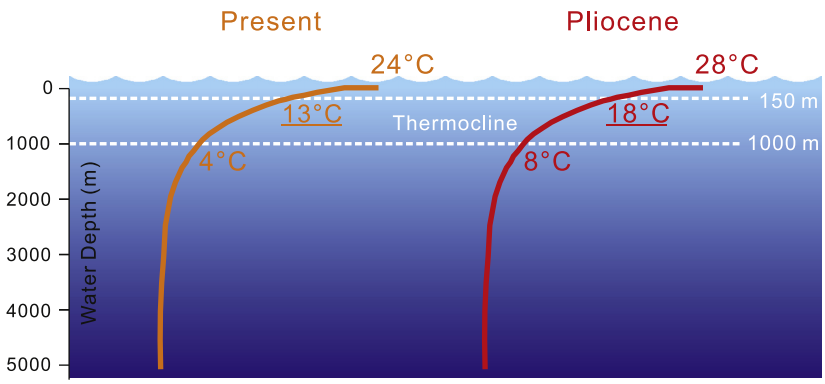

Fig. 5. Comparisons of the idealized temperature–depth relationship in the water column of EEP between the Pliocene (right) and the present (left). The Pliocene temperature profile is derived by a uniformly 4 °C warming in the surface (cf. Dekens et al., 2007; Lawrence et al., 2006; Rousselle et al., 2013; Zhang et al., 2014), subsurface (cf. Ford et al., 2012) and bottom waters (cf. Lear et al., 2015).

transition between warmer mixed-layer and cooler deep water, or the "thermocline", should no longer be defined as 13 °C, because the entire water column is shifted towards warmer temperatures (Fig. 5). Therefore, we argue against the interpretations of warmer subsurface temperatures in the ancient EEP (Ford et al., 2012) or elsewhere (Ford et al., 2015) as a sign of a deeper thermocline. Indeed, a relatively shallow EEP thermocline during late Miocene – Pliocene (Fig. 5) is implicated by high biogenic MARs as well as the appearance of CO_2 disequilibrium — all of which require upwelling of subsurface, thermoclinal waters. Warm thermoclinal waters of the Miocene–Pliocene EEP could have resulted from warmer extratropical source waters due to the substantially reduced meridional temperature gradient, as recently suggested (Zhang et al., 2014) and supported by subsequent studies (Fedorov et al., 2015; Ma et al., 2015).

Our $\varepsilon_{p37:2}$ and pCO_2 data confirm the existence of equatorial upwelling of deep-waters in the eastern Pacific Ocean during the warmer geological past. However, the interpretation of intensified upwelling from the CO_2 disequilibrium and nutrient supply is complicated by the possibility that ancient upwelled water contained higher nutrient and CO_2 levels relative to today. Deep waters could be older than modern conditions due to differences in source water pathways or locations, and/or enhanced global ocean nutrient content (Filippelli, 2008; Hermoyian and Owen, 2001), all of which could have led to higher export production and higher deep-water nutrient and CO_2 contents.

The "biogenic bloom" recorded in the EEP is consistent with the appearance of elevated export production rates across major upwelling systems elsewhere (Dickens and Owen, 1999; Diester-Haass et al., 2005; Farrell et al., 1995), and possibly in some oligotrophic regions (Hermoyian and Owen, 2001). Indeed, a period of elevated productivity appears to be a widely-distributed phenomenon characterized by a negative shift in benthic $\delta^{13}C$ values (~0.5–1.5‰) (Grant and Dickens, 2002), while upwelling systems experienced enhanced accumulation of biogenic sediments including opal (Cortese et al., 2004; Farrell et al., 1995), carbonate (Diester-Haass et al., 2005; Farrell et al., 1995; Grant and Dickens, 2002), and phosphorous (Filippelli, 2008; Hermoyian and Owen, 2001). Also, shifts in planktonic and benthic foraminiferal faunal assemblages indicative of high productivity (Dickens and Owen, 1999; Diester-Haass et al., 2005) and lower deep-water redox conditions (Dickens and Owen, 1999) support this interpretation. However, recent geochemical and geological evidences suggest that global continental weathering and erosion rates, the processes important for the supply of major nutrients (e.g., phosphorous) to the ocean, were not higher during the late Miocene – early Pliocene (Herman et al., 2013; Willenbring and von Blanckenburg, 2010). This implies that nutrient redistribution as exemplified by an opal sedimentation shift from the Atlantic Ocean to Indo-Pacific regions (Cortese et al., 2004; Dickens and Owen, 1999), and perhaps also enhanced mixing, are important for the "biogenic bloom". Regardless, evidence for persistent EEP upwelling suggests that the physical processes responsible for wind-driven deep-water upwelling and CO_2 disequilibrium, including a robust Walker circulation, a tilted and dynamic sea-level height and thermocline depth across the equatorial Pacific were all in operation for the past ~6.5 million years, with implications for our future climate in a high CO_2 world.

Acknowledgements

This study used samples and data provided by the International Ocean Discovery Program (IODP). Funding was provided by NSF AGS P2C2 award 1203163 to M.P., Royal Swedish Academy of Sciences through a grant from the Knut and Alice Wallenberg Foundation KAW 2009.0287 to J.H., and the Schlanger Ocean Drilling Fellowship to Y.G.Z. We thank Ellen Thomas for helpful discussions, Brad Erkkila and Glendon Husinger of the Yale Analytical and Stable Isotope Center for their technical support. Data from Site 850 and 806 can be found in the supplemental data table accompanying this paper. We thank Jerry Dickens and anonymous reviewers for their thoughtful reviews. We dedicate this article to the late Mark Pagani who was very enthusiastic about our studies in the tropical Pacific and an inspiring contributor to critical, scientific debate.

Appendix A. Supplementary material

Supplementary material related to this article can be found online at http://dx.doi.org/10.1016/j.epsl.2017.03.016.

References

Bakker, D.C.E., Pfeil, B., Smith, K., Hankin, S., Olsen, A., Alin, S.R., Cosca, C., Harasawa, S., Kozyr, A., Nojiri, Y., O'Brien, K.M., Schuster, U., Telszewski, M., Tilbrook, B., Wada, C., Akl, J., Barbero, L., Bates, N.R., Boutin, J., Bozec, Y., Cai, W.J., Castle, R.D., Chavez, F.P., Chen, L., Chierici, M., Currie, K., de Baar, H.J.W., Evans, W., Feely, R.A., Fransson, A., Gao, Z., Hales, B., Hardman-Mountford, N.J., Hoppema, M., Huang, W.J., Hunt, C.W., Huss, B., Ichikawa, T., Johannessen, T., Jones, E.M., Jones, S.D., Jutterström, S., Kitidis, V., Körtzinger, A., Landschützer, P., Lauvset, S.K., Lefèvre, N., Manke, A.B., Mathis, J.T., Merlivat, L., Metzl, N., Murata, A., Newberger, T., Omar, A.M., Ono, T., Park, G.H., Paterson, K., Pierrot, D., Ríos, A.F., Sabine, C.L., Saito, S., Salisbury, J., Sarma, V.V.S.S., Schlitzer, R., Sieger, R., Skjelvan, I., Steinhoff, T., Sullivan, K.F., Sun, H., Sutton, A.J., Suzuki, T., Sweeney, C., Takahashi, T., Tjiputra, J., Tsurushima, N., van Heuven, S.M.A.C., Vandemark, D., Vlahos, P., Wallace, D.W.R., Wanninkhof, R., Watson, A.J., 2014. An update to the Surface Ocean CO_2 Atlas (SOCAT version 2). Earth Syst. Sci. Data 6, 69–90.

Baldauf, J.G., Iwai, M., 1995. 7. Neogene diatom biostratigraphy for the eastern equatorial Pacific Ocean, Leg 138. In: Pisias, N.G., Mayer, L.A., Janecek, T.R., Palmer-Julson, A., van Andel, T.H. (Eds.), Proceedings of the Ocean Drilling Program, Scientific Results. Ocean Drilling Program, College Station, TX, pp. 105–128.

Benthien, A., Andersen, N., Schulte, S., Muller, P.J., Schneider, R.R., Wefer, G., 2002. Carbon isotopic composition of the $C_{37:2}$ alkenone in core top sediments of the South Atlantic Ocean: effects of CO_2 and nutrient concentrations. Glob. Biogeochem. Cycles 16.

Bidigare, R.R., Fluegge, A., Freeman, K.H., Hanson, K.L., Hayes, J.M., Hollander, D., Jasper, J.P., King, L.L., Laws, E.A., Milder, J., Millero, F.J., Pancost, R., Popp, B.N., Steinberg, P.A., Wakeham, S.G., 1997. Consistent fractionation of ^{13}C in nature and in the laboratory: growth-rate effects in some haptophyte algae. Glob. Biogeochem. Cycles 11, 279–292.

Bidigare, R.R., Hanson, K.L., Buesseler, K.O., Wakeham, S.G., Freeman, K.H., Pancost, R.D., Millero, F.J., Steinberg, P.A., Popp, B.N., Latasa, M., Landry, M.R., Laws, E.A., 1999. Iron-stimulated changes in ^{13}C fractionation and export by equatorial Pacific phytoplankton: toward a paleogrowth rate proxy. Paleoceanography 14, 589–595.

Bjerknes, J., 1969. Atmospheric teleconnections from the equatorial Pacific. Mon. Weather Rev. 97, 163–172.

Brierley, C.M., Fedorov, A.V., Liu, Z.H., Herbert, T.D., Lawrence, K.T., LaRiviere, J.P., 2009. Greatly expanded tropical warm pool and weakened Hadley circulation in the early Pliocene. Science 323, 1714–1718.

Chaisson, W.P., Leckie, R.M., 1993. 10. High-resolution Neogene planktonic foraminifer biostratigraphy of Site 806, Ontong Java Plateau (western equatorial Pacific). In: Berger, W.H., Kroenke, L.W., Mayer, L.A. (Eds.), Proc. ODP, Sci. Results. Ocean Drilling Program, College Station, TX, pp. 137–178.

Coale, K.H., Fitzwater, S.E., Gordon, R.M., Johnson, K.S., Barber, R.T., 1996. Control of community growth and export production by upwelled iron in the equatorial Pacific Ocean. Nature 379, 621–624.

Conte, M., Thompson, A., Eglinton, G., Green, J.C., 1995. Lipid biomarker diversity in the coccolithophorid *Emiliania huxleyi* (Prymnesiophyceae) and the related species *Gephyrocapsa oceanica*. J. Phycol. 31, 272–282.

Cortese, G., Gersonde, R., Hillenbrand, C.-D., Kuhn, G., 2004. Opal sedimentation shifts in the World Ocean over the last 15 Myr. Earth Planet. Sci. Lett. 224, 509–527.

Dekens, P.S., Ravelo, A.C., McCarthy, M.D., 2007. Warm upwelling regions in the Pliocene warm period. Paleoceanography 22, PA3211.

Deutsch, C., Berelson, W., Thunell, R., Weber, T., Tems, C., McManus, J., Crusius, J., Ito, T., Baumgartner, T., Ferreira, V., Mey, J., van Geen, A., 2014. Centennial changes in North Pacific anoxia linked to tropical trade winds. Science 345, 665–668.

Dickens, G.R., Owen, R.M., 1999. The latest Miocene – early Pliocene biogenic bloom: a revised Indian Ocean perspective. Mar. Geol. 161, 75–91.

Diester-Haass, L., Billups, K., Emeis, K.-C., 2005. In search of the late Miocene–early Pliocene "biogenic bloom" in the Atlantic Ocean (Ocean Drilling Program Sites 982, 925 and 1088). Paleoceanography 20.

DiNezio, P.N., Clement, A.C., Vecchi, G.A., 2010. Reconciling differing views of tropical Pacific climate change. Eos Trans. AGU 91, 141–142.

Eek, M., Whiticar, M.J., Bishop, J.K.B., Wong, C.S., 1999. Influence of nutrients on carbon isotope fractionation by natural populations of Prymnesiophyte algae in NE Pacific. Deep-Sea Res., Part 2, Top. Stud. Oceanogr. 46, 2863–2876.

Farrell, J.W., Raffi, I., Janecek, T.R., Murray, D.W., Levitan, M., Dadey, K.A., Emeis, K.-C., Lyle, M., Flores, J.-A., Hovan, S., 1995. 35. Late Neogene sedimentation patterns in the eastern equatorial Pacific Ocean. In: Pisias, N., Mayer, L., Janecek, T., Palmer-Julson, A., van Andel, T.H. (Eds.), Proceedings of the Ocean Drilling Program, Scientific Results. Ocean Drilling Program, College Station, TX.

Fedorov, A.V., Brierley, C.M., Lawrence, K.T., Liu, Z., Dekens, P.S., Ravelo, A.C., 2013. Patterns and mechanisms of early Pliocene warmth. Nature 496, 43–49.

Fedorov, A.V., Burls, N.J., Lawrence, K.T., Peterson, L.C., 2015. Tightly linked zonal and meridional sea surface temperature gradients over the past five million years. Nat. Geosci. 8, 975–980.

Fedorov, A.V., Dekens, P.S., McCarthy, M., Ravelo, A.C., deMenocal, P.B., Barreiro, M., Pacanowski, R.C., Philander, S.G., 2006. The Pliocene Paradox (mechanisms for a permanent El Nino). Science 312, 1485–1489.

Feely, R.A., Boutin, J., Cosca, C.E., Dandonneau, Y., Etcheto, J., Inoue, H.Y., Ishii, M., Le Quere, C., Mackey, D.J., McPhaden, M.J., Metzl, N., Poisson, A., 2002. Seasonal and interannual variability of CO_2 in the equatorial Pacific. Deep-Sea Res., Part 2, Top. Stud. Oceanogr. 49, 2443–2469.

Fiedler, P.C., Talley, L.D., 2006. Hydrography of the eastern tropical Pacific: a review. Prog. Oceanogr. 69, 143–180.

Filippelli, C.M., 2008. The global phosphorus cycle: past, present and future. Elements 4, 89–95.

Ford, H.L., Ravelo, A.C., Hovan, S., 2012. A deep Eastern Equatorial Pacific thermocline during the early Pliocene warm period. Earth Planet. Sci. Lett. 355–356, 152–161.

Ford, H.L., Ravelo, A.C., Dekens, P.S., LaRiviere, J., Wara, M.W., 2015. The evolution of the equatorial thermocline and the early Pliocene *El Padre* mean state. Geophys. Res. Lett. 42, 4878–4887.

Freeman, K.H., Pagani, M., 2005. Alkenone-based estimates of past CO_2 levels: a consideration of their utility based on an analysis of uncertainties. In: Ehleringer, J.R., Cerling, T.E., Dearing, M.D. (Eds.), A History of Atmospheric CO_2 and Its Effects on Plants, Animals, and Ecosystems. Springer, New York.

Goericke, R., Montoya, J.P., Fry, B., 1994. Physiology of isotope fractionation in algae and cyanobacteria. In: Lajtha, K., Michener, B. (Eds.), Stable Isotope in Ecology. Blackwell Scientific, Cambridge, pp. 187–221.

Goericke, R., Welschmeyer, N.A., 1998. Response of Sargasso Sea phytoplankton biomass, growth rates and primary production to seasonally varying physical forcing. J. Plankton Res. 20, 2223–2249.

Grant, K.M., Dickens, G.R., 2002. Coupled productivity and carbon isotope records in the southwest Pacific Ocean during the late Miocene – early Pliocene biogenic bloom. Palaeogeogr. Palaeoclimatol. Palaeoecol. 187, 61–82.

Henderiks, J., 2008. Coccolithophore size rules – reconstructing ancient cell geometry and cellular calcite quota from fossil coccoliths. Mar. Micropaleontol. 67, 143–154.

Henderiks, J., Pagani, M., 2007. Refining ancient carbon dioxide estimates: significance of coccolithophore cell size for alkenone-based pCO_2 records. Paleoceanography, 22.

Herman, F., Seward, D., Valla, P.G., Carter, A., Kohn, B., Willett, S.D., Ehlers, T.A., 2013. Worldwide acceleration of mountain erosion under a cooling climate. Nature 504, 423–426.

Hermoyian, C.S., Owen, R.M., 2001. Late Miocene–early Pliocene biogenic bloom: evidence from low-productivity regions of the Indian and Atlantic Oceans. Paleoceanography 16, 95–100.

Hovan, S.A., 1995. 28. Late Cenozoic atmospheric circulation intensity and climatic history recorded by eolian deposition in the eastern equatorial Pacific Ocean, Leg 138. In: Pisias, N., Mayer, L., Janecek, T., Palmer-Julson, A., van Andel, T.H. (Eds.), Proceedings of the Ocean Drilling Program, Scientific Results. Ocean Drilling Program, College Station, TX, pp. 615–625.

Jasper, J.P., Hayes, J.M., Mix, A.C., Prahl, F.G., 1994. Photosynthetic fractionation of ^{13}C and concentrations of dissolved CO_2 in the central equatorial Pacific during the last 255,000 years. Paleoceanography 9, 781–798.

Keeling, C.D., 1968. Carbon dioxide in surface ocean waters: 4. Global distribution. J. Geophys. Res. 73, 4543–4553.

Keller, K.M., Joos, F., Lehner, F., Raible, C.C., 2015. Detecting changes in marine responses to ENSO from 850–2100 CE: insights from the ocean carbon cycle. Geophys. Res. Lett. 42.

Lawrence, K.T., Liu, Z.H., Herbert, T.D., 2006. Evolution of the Eastern Tropical Pacific through Plio-Pleistocene glaciation. Science 312, 79–83.

Laws, E.A., Popp, B.N., Bidigare, R.R., Riebesell, U., Burkhardt, S., Wakeham, S.G., 2001. Controls on the molecular distribution and carbon isotopic composition of alkenones in certain haptophyte algae. Geochem. Geophys. Geosyst. 2.

Lear, C.H., Coxall, H.K., Foster, G.L., Lunt, D.J., Mawbey, E.M., Rosenthal, Y., Sosdian, S., Thomas, E., Wilson, P.A., 2015. Neogene ice volume and ocean temperatures: insights from infaunal foraminiferal Mg/Ca paleothermometry. Paleoceanography 2015, 1437–1454.

Lyle, M., 2003. Neogene carbonate burial in the Pacific Ocean. Paleoceanography 18.

Ma, Z., Ravelo, A.C., Liu, Z., Zhou, L., Paytan, A., 2015. Export production fluctuations in the eastern equatorial Pacific during the Pliocene–Pleistocene: reconstruction using barite accumulation rates. Paleoceanography 30, 1455–1469.

Martinez-Boti, M.A., Marino, G., Foster, G.L., Ziveri, P., Henehan, M.J., Rae, J.W.B., Mortyn, P.G., Vance, D., 2015. Boron isotope evidence for oceanic carbon dioxide leakage during the last deglaciation. Nature 518, 219–222.

McPhaden, M.J., Zebiak, S.E., Glantz, M.H., 2006. ENSO as an integrating concept in Earth Science. Science 314, 1740–1745.

Nathan, S.A., Leckie, R.M., 2009. Early history of the Western Pacific Warm Pool during the middle to late Miocene (~13.2–5.8 Ma): role of sea-level change and implications for equatorial circulation. Palaeogeogr. Palaeoclimatol. Palaeoecol. 274, 140–159.

O'Brien, C.L., Foster, G.L., Martinez-Boti, M.A., Abell, R., Rae, J.W.B., Pancost, R.D., 2014. High sea surface temperatures in tropical warm pools during the Pliocene. Nat. Geosci. 7, 606–611.

O'Connor, B.M., Fine, R.A., Maillet, K.A., Olson, D.B., 2002. Formation rates of subtropical underwater in the Pacific Ocean. Deep-Sea Res., Part 1, Oceanogr. Res. Pap. 49, 1571–1590.

Pagani, M., 2014. 12.13 Biomarker-based inferences of past climate: the alkenone pCO_2 proxy. In: Holland, H.D., Turekian, K.K. (Eds.), Treatise on Geochemistry. Elsevier, Oxford, pp. 361–378.

Pagani, M., Freeman, K.H., Arthur, M.A., 1999. Late Miocene atmospheric CO_2 concentrations and the expansion of C_4 grasses. Science 285, 876–879.

Pagani, M., Liu, Z.H., LaRiviere, J., Ravelo, A.C., 2010. High Earth-system climate sensitivity determined from Pliocene carbon dioxide concentrations. Nat. Geosci. 3, 27–30.

Pagani, M., Zachos, J.C., Freeman, K.H., Tipple, B., Bohaty, S., 2005. Marked decline in atmospheric carbon dioxide concentrations during the Paleogene. Science 309, 600–603.

Palmer, M.R., Pearson, P.N., 2003. A 23,000-year record of surface water pH and pCO_2 in the western equatorial Pacific Ocean. Science 300, 480–482.

Philander, S.G., Fedorov, A.V., 2003. Role of tropics in changing the response to Milankovich forcing some three million years ago. Paleoceanography 18, 1045.

Popp, B.N., Hanson, K.L., Dore, J.E., Bidigare, R.R., Laws, E.A., Wakeham, S.G., 1999. Controls on the carbon isotopic composition of phytoplankton: paleoceanographic perspectives. In: Abrantes, F., Mix, A.C. (Eds.), Reconstructing Ocean History: A Window into the Future. Plenum Publishers, New York, pp. 381–398.

Prahl, F.G., Dymond, J., Sparrow, M.A., 2000. Annual biomarker record of export production in the central Arabian Sea. Deep-Sea Res., Part 2, Top. Stud. Oceanogr. 47, 1584–1604.

Raffi, I., Flores, J.-A., 1995. Pleistocene through Miocene calcareous nannofossils from eastern equatorial Pacific Ocean (Leg 138). In: Pisias, N., Mayer, L., Janecek, T., Palmer-Julson, A., van Andel, T.H. (Eds.), Proceedings of the Ocean Drilling Program, Scientific Results. Ocean Drilling Program, College Station, TX, pp. 105–128.

Reghellin, D., Coxall, H.K., Dickens, G.R., Rackman, J., 2015. Carbon and oxygen isotopes of bulk carbonate in sediment deposited beneath the eastern equatorial Pacific over the last 8 million years. Paleoceanography 30, 1261–1286.

Rommerskirchen, F., Condon, T., Mollenhauer, G., Dupont, L., Schefuss, E., 2011. Miocene to Pliocene development of surface and subsurface temperatures in the Benguela Current system. Paleoceanography 26.

Rosell-Mele, A., Martinez-Garcia, A., McClymont, E.L., 2014. Persistent warmth across the Benguela upwelling system during the Pliocene epoch. Earth Planet. Sci. Lett. 386, 10–20.

Rousselle, G., Beltran, C., Sicre, M.-A., Raffi, I., De Rafelis, M., 2013. Changes in sea-surface conditions in the Equatorial Pacific during the middle Miocene–Pliocene as inferred from coccolith geochemistry. Earth Planet. Sci. Lett. 361, 412–421.

Schroeder, J.O., Murray, R.W., Leinen, M., Pflaum, R.C., Janecek, T.R., 1997. Barium in equatorial Pacific carbonate sediment: terrigenous, oxide, and biogenic associations. Paleoceanography 12, 125–146.

Seki, O., Foster, G.L., Schmidt, D.N., Mackensen, A., Kawamura, K., Pancost, R.D., 2010. Alkenone and boron-based Pliocene pCO_2 records. Earth Planet. Sci. Lett. 292, 201–211.

Serno, S., Winckler, G., Anderson, R.F., Hayes, C.T., Ren, H., Gersonde, R., Haug, G.H., 2014. Using the natural spatial pattern of marine productivity in the Subarctic North Pacific to evaluate paleoproductivity proxies. Paleoceanography 29, 438–453.

Shackleton, N.J., Crowhurst, S., Hagelberg, T., Pisias, N.G., Schneider, D.A., 1995. A new late Neogene time scale: application to Leg 138 sites. In: Pisias, N.G., Mayer, L.A., Janecek, T.R., Palmer-Julson, A., van Andel, T.H. (Eds.), Proceedings of the Ocean Drilling Program, Scientific Results. Ocean Drilling Program, College Station, TX.

Shackleton, N.J., Hall, M.A., 1995. Stable isotopes records in bulk sediments (Leg 138). In: Pisias, N.G., Mayer, L.A., Janecek, T., Palmer-Julson, A., van Andel, T.H. (Eds.), Proceedings of the Ocean Drilling Program, Scientific Results. Ocean Drilling Program, College Station, TX.

Shipboard Scientific Party, 1991. 8. Site 806. In: Kroenke, L.W., Berger, W.H., Janecek, T. (Eds.), Proc. ODP, Init. Repts. Ocean Drilling Program, College Station, TX, pp. 291–367.

Shipboard Scientific Party, 1992. Site 850. In: Mayer, L., Pisias, N., Janecek, T. (Eds.), Proc. ODP, Init. Repts. Ocean Drilling Program, College Station, pp. 809–889.

Sucheras-Marx, B., Henderiks, J., 2014. Downsizing the pelagic carbon factory: impacts of calcareous nannoplankton evolution on calcareous nannoplankton evolution on carbonate burial over the past 17 million years. Glob. Planet. Change 123, 97–109.

Sutton, A.J., Feely, R.A., Sabine, C.L., McPhaden, M.J., Takahashi, T., Chavez, F.P., Friederich, G.E., Mathis, J.T., 2014. Natural variability and anthropogenic change in equatorial Pacific surface ocean pCO_2 and pH. Glob. Biogeochem. Cycles 28, 2013GB004679.

Takahashi, T., Sutherland, S.C., 2012. Global Ocean Surface Water Partial Pressure of CO_2 Database: Measurements Performed During 1957–2012. U.S. Department of Energy, Carbon Dioxide Information Analysis Center, Oak Ridge National Laboratory, Oak Ridge, TN, pp. 1–13.

Takahashi, T., Sutherland, S.C., Wanninkhof, R., Sweeney, C., Feely, R.A., Chipman, D.W., Hales, B., Friederich, G., Chavez, F., Sabine, C., Watson, A., Bakker, D.C.E., Schuster, U., Metzl, N., Yoshikawa-Inoue, H., Ishii, M., Midorikawa, T., Nojiri, Y., Körtzinger, A., Steinhoff, T., Hoppema, M., Olafsson, J., Arnarson, T.S., Tilbrook, B., Johannessen, T., Olsen, A., Bellerby, R., Wong, C.S., Delille, B., Bates, N.R., de Baar, H.J.W., 2009. Climatological mean and decadal change in surface ocean pCO_2, and net sea–air CO_2 flux over the global oceans. Deep-Sea Res., Part 2, Top. Stud. Oceanogr. 56, 554–577.

Takayama, T., 1993. 11. Notes on Neogene calcareous nannofossil biostratigraphy of the Ontong Java Plateau and size variations of *Reticulofenestra* coccoliths. In: Berger, W.H., Kroenke, L.W., Mayer, L. (Eds.), Proceedings of the Ocean Drilling Program, Scientific Results. Ocean Drilling Program, College Station, TX, pp. 179–229.

Willenbring, J.K., von Blanckenburg, F., 2010. Long-term stability of global erosion rates and weathering during the late-Cenozoic cooling. Nature 465, 211–214.

Zhang, Y.G., Pagani, M., Liu, Z., 2014. A 12-million-year temperature history of the tropical Pacific Ocean. Science 343, 84–87.